Powder Technology 364 (2020) 738–745

Contents lists available at ScienceDirect

Powder Technology

journal homepage: www.elsevier.com/locate/powtec

Aerosol aggregation through modulated symmetrically opposing acoustic field in normal 16-sided waveguide coupled with resonators

Zhenghui Qiao [a,b,*], Shaohua Liang [a], Xiaojun Pan [a], Xiaolong Bi [a], Siwen Zhang [a], Caixia Bian [a], Haiming Gu [a], Linghai Chen [a], Mei Cheng [b,d], Yawei Jin [b], Suya Shi [a], Dianjia Zhu [c]

[a] College of Energy and Power Engineering, Nanjing Institute of Technology, Nanjing 211167, China
[b] Key Laboratory of Energy Thermal Conversion and Control of Ministry of Education, School of Energy and Environment, Southeast University, Nanjing 210096, China
[c] Display Research center, Southeast University, Nanjing 210096, China
[d] Engineering Management Department, Jiangsu Heng Rui Medicine Co, . LTD, Lianyungang, Jiangsu Province 222047, China

ARTICLE INFO

Article history:
Received 18 September 2019
Received in revised form 1 February 2020
Accepted 11 February 2020
Available online xxxx

Keywords:
Aerosol
Acoustic field
Aggregation
$PM_{2.5}$
Nanoparticles
Manipulation

ABSTRACT

Aerosol control is a big revolution in production and use of submicronic particles. Developing a novel aerosol control technology in the area is the study objective of this paper. Attributing to the aerosol control potential in acoustics, a normal 16-sided aerosol aggregation chamber (pelletier dish) symmetrically installed with 16 poles of Helmholtz sound source (HSS) is successfully used to aggregate smog aerosols. The aerosols are generated by the combustion of chemical material. In the acoustic conditions of 2, 4, 8 and 16 beams of opposing waves, the shapes of aerosol distribution always display as the specific aerosol petals of number equaling to the operating number of HSS. With the increase of the operating number, the removal effectiveness rises gradually to 1.5 wavelengths, obviously larger than half wavelengths achieved in the previous study. The results are repeatability in experiment, and especially the aerosol aggregation can be pre-designed by acoustic field simulation.

1. Introduction

It is internationally agreed that aerosol control is a big revolution in production and use of particulate matter [1]. Aerosol /particle emission are even present in electronics and cosmetics. Many other sectors for example polymeric composite materials are carrying out a lot of scientific and technological works. However, recent works on particle emission introduced in thin layer showcase potential risks of aerosol releases and allow a more balanced benefit/risk analysis. For example, many studies highlight nanoparticle emissions due to coatings, paints [2], tiles [3]. Cases of nanoparticle exposure in the field of occupational hygiene at coating workplaces have been reported [4]. These aspects should be addressed on the basis of the future progress of aerosol control technique. Developing one new aerosol technology in the area is the study objective of this paper.

Aerosol such as the chemical smog belongs to the common non-negligible type of air pollution source. One main component of smog aerosol is particulate matter of size no larger than 2.5 μm ($PM_{2.5}$). Taking the societal role of engineers as an example, the 'first, do not harm' approach, a tradition in medicine, seems not to be the consensus in engineering [3]. The massive and direct emission of such aerosol can cause serious challenge of atmosphere and the health [5,6]. The specific scenarios include the environmental release [1], the release to the worker (occupational risk [7]), and the release to the consumer (health risk [8]). Attributing to the potential utilization value of wave energy [9–11], different types of acoustic field [12–21] are constructed to aggregate different kinds of aerosols. The acoustics-aerosol studies [19–27] contribute to the development of aerosol removal technique [12,28].

A series research about aerosol acoustic aggregation has been recently carried out in detail. For example, Zhang's team [12] verifies the regulation range (75% ~ 85%) of the additional particles on the acoustic agglomeration efficiency of coal-fired fly-ash particles (1–10 μm). Their study [29] indicates the elimination feasibility of acoustic frequency (1.5 kHz) and sound pressure level (141 dB) on fire smokes. In expressing the agglomeration mechanism, different from Zhang's agglomeration model [30], Wei's team [31] proposes a practicable agglomeration model for multi-phase fluid of droplet aerosol. The model simulation is appropriate to the case in high temperature and high pressure environment. Zheng's team [32] verifies the influence of different size fine particles on acoustic agglomeration mechanism selection. Yan's team [33] verifies the tuning effect of seed nuclei on acoustic fine particles removal, and the tuning range of removal efficiency is 53% ~ 80% [28]. Shen's team [13] verifies the regulation range (36% to 52%) of the

* Corresponding author at: College of Energy and Power Engineering, Nanjing Institute of Technology, Nanjing 211167, China.
E-mail address: qiaozhenghui@njit.edu.cn (Z. Qiao).

https://doi.org/10.1016/j.powtec.2020.02.032
0032-5910/

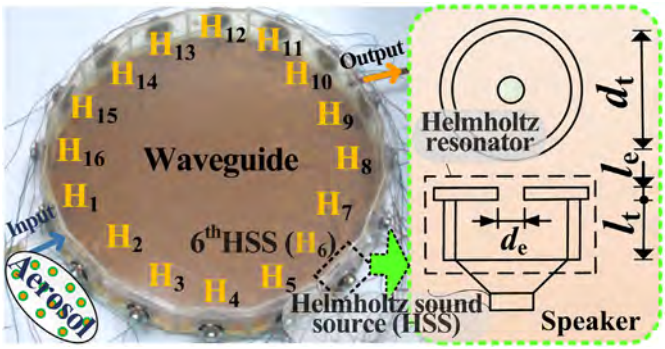

Fig. 1. Schematic diagram of setup.

spraying method on the removal efficiency of particles (< 10 μm). Kristina [34] develops a new acoustic chamber used for more efficiently agglomerating small diameter particles (0.3–10 μm) within diesel engine exhaust. These studies demonstrate that the appropriate aggregation chamber, the acoustic aggregation tuning, the aggregation mechanism and the utilized aerosol type are very important in the aerosol removal area, but still face challenges. In order to achieve a comprehensive aerosol aggregation effect, the aspects of study objective here relate to above challenges.

For the challenge of aggregation chamber, the one-dimensional waveguide used for generating one-dimensional acoustic field is generally selected in the current studies [12,13,15–17,20,22,28]. In contrast, it is only recently realized that the two-dimensional waveguide used for generating two-dimensional acoustic field has potential advantage in industrially designing huge aerosol apparatus [19]. The aggregation chamber (waveguide) of two dimensions should be studied further. Compare to a smaller number of sound sources generally used (such as one source [29,35], two Helmholtz sound sources (HSS) [15,17]), the installation of multiple sound sources allows more conveniently for the manufacture of large-scale aerosol device [19]. Therefore, the installation method of multiple HSS is focused here. For the challenge of acoustic aggregation tuning, the engineering advantage of multiple acoustic wave-packet [17], phase-control [19], temperature tuning [15] and resonance mode [16] on aerosol aggregation has been verified. However, aerosol aggregation process tuning depended on the operating number change of multiple sound sources needs to be focused to enrich the tuning method. For the aggregation mechanism, besides the different kinds of agglomeration kernel mechanisms [29], the mechanism of acoustic radiation force should be focused [17], especially in the two-dimension acoustic field of Bessel beams [36]. For the utilized aerosol type, instead of the previous fire smoke [29], tobacco smoke [17], coal-fired fly-ash particles [23] and diesel engine exhaust [15,34], the chemical smog aerosols is focused here to enlarge the aerosol scope of acoustic aggregation.

Accordingly, the aerosol technology studied in this paper is the smog aerosol aggregation tuning in normal 16-sided two-dimensional waveguide coupled with resonant sound sources of quantity 16. The study aspects are very exceptional and novel in powder technology.

Table 1
Four modes of operating condition.

Mode type	Number of poles	The positions of HSS							
		(1,9)	(2,10)	(3,11)	(4,12)	(5,13)	(6,14)	(7,15)	(8,16)
1	$2 = 2^1$	+	−	−	−	−	−	−	−*
2	$4 = 2^2$	+	−	−	−	+	−	−	−
3	$8 = 2^3$	+	−	+	−	+	−	+	−
4	$16 = 2^4$	+	+	+	+	+	+	+	+

* '+' and '- ' respectively indicate open and closed states of HSS.

The energy-motivated type of aerosol aggregation belongs to the no-uniform two-dimensional acoustic standing wave field modulated by tuning pair number of symmetrically opposing HSS. This study reveals that the aerosol aggregation process can be sensitively controlled by the petal number of high concentration aerosol zone. The petal number equals to the operating number of multiple HSS. The aerosol petal distribution in two-dimensional aggregation chamber can be designed by acoustic field pre-simulation. The findings and methodology are a valuable contribution to the area, a topic which occupies and will occupy generations of researchers, particularly in the field of submicronic particles.

2. Experiment and method

2.1. Experimental setup

Fig. 1 shows the acoustic coupling device with one regular waveguide and sixteen HSS. Around the center of waveguide, eight pairs of same opposing HSS are symmetrically assembled on side center of regular polygon cavity with 16 edges. One HSS is composed of Helmholtz resonator (HR) and electro-magnetic speaker. The diameter of the internally tangent circle is 480 mm. The size of device satisfies the similarity condition of resonance [17],

$$\left(\frac{nc_0}{2L_n}\right)^2 = \left(\frac{c_0^2}{4\pi^2}\right)\left(\frac{\pi d_e^2}{(l_e + 0.73d_e)\left(l_t \pi d_t^2\right)}\right) = f_0^2 \tag{1}$$

Here $n = 5$ is the harmonic order of waveguide; $L_n = 48$ cm is the distance of two opposing HSS; c_0 is the sound velocity of air; $d_e = 8$ mm, $l_e = 4.5$ mm, $l_t = 4.5$ mm and $d_t = 35$ mm are the geometric size of HR; $f_0 = 1.805$ kHz is resonance frequency of HR, and also equals to the fifth order harmonic frequency of waveguide. With the input frequency $f_0 = c_0/\lambda$ of electric signal for speaker, the setup works at the acoustic state of resonance. $\lambda = 192$ mm is the wavelength of acoustic wave. For generating two-dimensional acoustic standing wave field, the height (60 mm) of waveguide should be less than half-wavelength. In the horizontal direction of waveguide, the dimension parameter of set-up can be changed. The value ranges of all parameters must satisfy Eq. 1, which can be used to design the size and frequency parameters of the large-scale aerosol device in future industrial manufacture.

In the counterclockwise direction, each sign of H_i (i is integer) stamps each HSS. A pair of opposing HSS consists of two opposing HSS, such as the first pair including H_1 and H_9, abbreviated as (1,9). The total number of pairs is eight, and each pair is shown in Table 1. For generating symmetrically opposing acoustic field with high quality [37,38], arbitrary two opposing HSS is demonstrated as one whole unit including two poles of sources, and their phase equals π [19]. This single unit is stamped as the position array of HSS. Based on the symmetrically opposing principle of synthetic standing wave field [17], there exist different operating conditions with four types of modes. The series of mode type is demonstrated as the index m of power operation 2^m that equals to the pole number of operating HSS. It should be note that these operating modes have not been focused in previous study.

In the experimental process, the input signal of speaker is the specific electric voltage of sinusoid with the frequency 1.805 kHz and the amplitude in range of 0.5–10 V. It is generally considered that the acoustic wave with the low frequency of 1.805 kHz similar to 1.286 kHz [17], 1.5 kHz [29] and 2.642 kHz [19] has specific advantage in smog aerosol aggregation. The sound pressure amplitude is about 60 Pa. The amplitude variation depends on the experimentally optimal aerosol aggregation effect. The maximum of low concentration aerosol area is selected as the parameter characterizing the optimal effect [17,19,38]. Chemical smog with main compounds of tetramethrin and three chlorine permethrin [19] is inhaled into waveguide to display aerosol aggregation

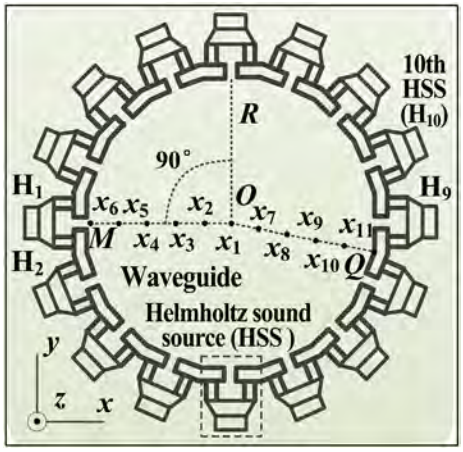

Fig. 2. Arrangement for the test points.

effect. The smog aerosol source is the specific combustion process of chemical material. The initial aerosol size distributions and the amount percents are of 0.3–0.5 μm for 56.25%, 0.5–1.0 μm for 18.7%, 1.0–2.5 μm for 16.24%, 2.5–5 μm for 6.34%, 5.0–10.0 μm for 2.02%, >10.0 μm for 0.45%. The aerosol characteristic data is measured out by the particle counter of type *PlantTower* I. The measured results are similar to the tobacco smoke material [17]. The experimental temperature is 25 °C.

2.2. Methods

2.2.1. Aggregation mechanism

For the no-uniform two-dimensional acoustic standing wave field, acoustic radiation force F^{rad} is generally applied to the aerosols of size much smaller than wave-length. Once the small smog particle equals to the compressible sphere, the F^{rad} of acoustic field on a single particle can be expressed as [39,40],

$$F^{rad} = -\left(\pi A^2 V_{pt}\beta_{fm}/(2\lambda)\right)\psi(\beta,\rho)\,\sin(2kx) \tag{2a}$$

$$\psi(\beta,\rho) = \frac{5\rho_{pt}-2\rho_{fm}}{2\rho_{pt}+\rho_{fm}} - \frac{\beta_{pt}}{\beta_{fm}} \tag{2b}$$

Here, A is the amplitude of sound pressure; V_{pt} is the volume of particle; ρ and β are respectively the compressible coefficient and density, and the subscripts of "pt" and "fm" represent respectively the particle and the fluid medium; k is the wave number; x is the position relating to the anti-node and node of standing wave. $\psi(\rho,\beta)$ is the acoustic contrast factor depended on the physical characteristic of particle and its surrounding fluid. Attributing to the practically complex particle characteristic of chemical smog and the regime of F^{rad}, for the aerosol of $\psi(\rho,\beta) > 0$, the particles are driven and accumulated to the node of standing wave; for the aerosol of $\psi(\rho,\beta) < 0$, the aerosol particles are driven and accumulated to the anti-node of standing wave.

2.2.2. Removal evaluation

In the action process of acoustic field, the aggregation performance at any moment can be evaluated by the removal efficiency. For each aerosol size range, the efficiency at certain moment can be weighed by Eq. 3,

$$\eta = \frac{C_{initial} - C_{moment}}{C_{initial}} \times 100\% \tag{3}$$

Here $C_{initial}$ is the initial aerosol number concentration; C_{moment} is the aerosol number concentration at other moment. With the acoustic sustained action, η weighs the aerosol concentration variation.

2.2.3. The analysis of acoustic field

For measuring the characteristic of acoustic field, 11 test points for the positions of acoustic sensor are shown in Fig. 2. The center of regular polygon with 16-sides is stamped as O, which is defined as the origin of three-dimensional Cartesian coordinate system x-y-z. The radiuses of the internally and externally tangent circles for the polygon are respectively stamped as the line segments of *OM* and *OQ*. The two segments are uniformly divided by 11 test points of x_1 to x_{11}. The distance of adjacent points is about one quarter of acoustic wavelength. Attributing to the symmetrical characteristic of regular polygon and the homogeny of 16 HSS, the measurement of sound pressure on the x-y plane can be simplified as the measurement on quarter plane *MOR* of 16-sides waveguide. Under the operating condition with one pair of opposing HSS, 4 test points on quarter plane can be equivalently detected by selecting different HSS pair, such as the operating alternation from H(1,9) to H(2,10). Using this method, the pressure distribution on quarter plane can be equivalently acquired by the divided test points on *OM* and *OQ*.

For conveniently evaluating the characteristic of acoustic field with different pairs of opposing HSS, the sound pressure distribution in space and time can be calculated. For the general consideration neglecting dissipation, the kernel equation of this calculation process is wave equation,

$$\left(\frac{\partial}{\partial x}j_x + \frac{\partial}{\partial y}j_y + \frac{\partial}{\partial z}j_z\right)^2 p + kp = 0 \tag{4}$$

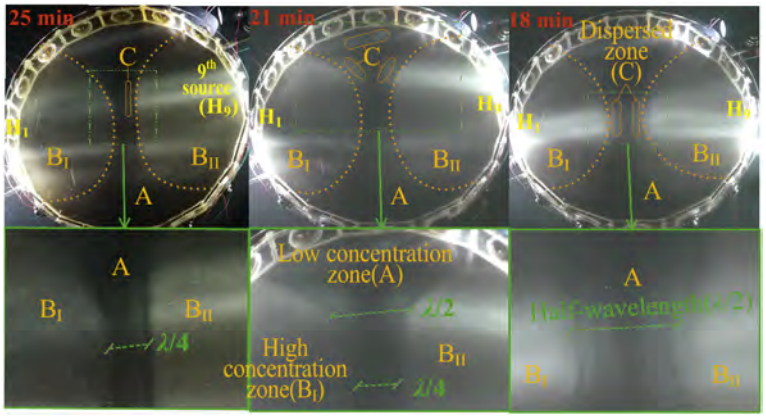

Fig. 3. The manipulation effect with one pair of resonators.

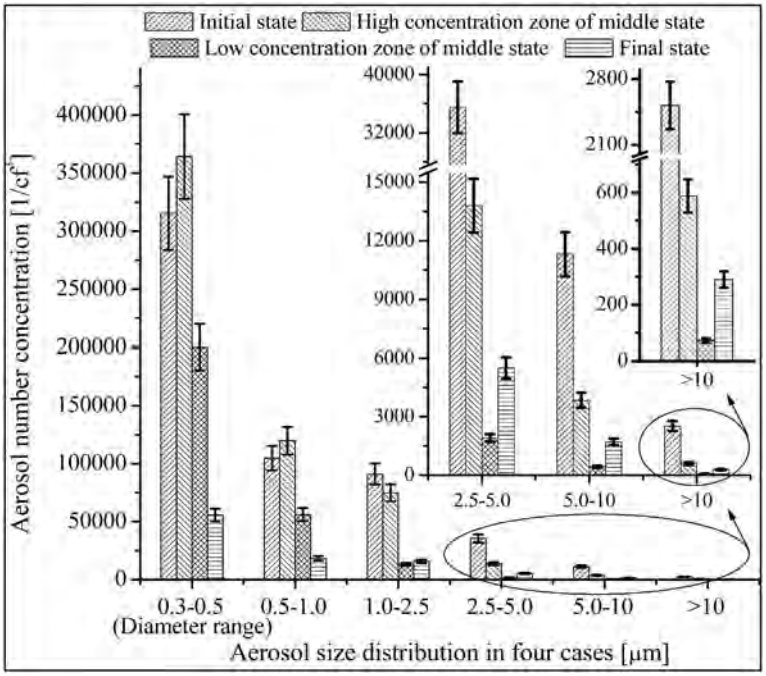

Fig. 4. The aerosol characteristic.

where k is wave number; $\boldsymbol{j}_x$, $\boldsymbol{j}_y$ and $\boldsymbol{j}_z$ are the unit direction vector of coordinate axis. Combing the point source type of boundary condition provided by Table 1, the complex aerosol-acoustics system with opposing HSS is predicable. Under different operating modes, the specific inhomogeneous acoustic field synthesized in waveguide can be simulated by using the scientific *Ansys* soft with the acoustic analysis model based on Eq. 4.

3. Results and analysis

3.1. The aggregation performance in operating mode 1

3.1.1. Aerosol concentration and removal efficiency

Fig. 3 shows experimentally the macro aggregation pattern in waveguide under the operating mode condition of two poles. The dark zone A in the middle of waveguide represents the low concentration zone. The bright zones B_I and B_{II} represent the high concentration zone. The boundaries between zone A and B constitute the pattern of "I" shape shown by arc curves in picture. With the sustained action of acoustic field, the gradually clear boundary curves demonstrate that the high and low concentration characteristic gradually become obvious. The dispersed C zones with high concentration in zone A gradually diminish. The pattern width in the ends of I shape is much larger than the width λ/4 of its middle. This characteristic length represents the size of aerosol removal within pattern I.

Fig. 4 quantifies the number concentration variation for each aerosol size range. The initial state corresponds to the beginning moment of device operation. The high and low concentration zones correspond to the middle state for the acoustic action of 23 min. The final state corresponds to the acoustic action of 50 min, close to the previous 56 min [17]. It can be seen that the final state concentrations for the size ranges of six are obviously less than the initial state concentrations. The aerosol numbers in the high concentration zone are also much less than those in the low concentration zone. For the aerosol size range about <1.0 μm, the aerosol numbers in the high concentration zone is seemingly larger than that in the initial state, while the aerosol numbers in the low concentration zone are less than that in the initial state. For the aerosol size range about >1.0 μm, the aerosol numbers in the low concentration zone are obviously less than that in the final state, even though the aerosol numbers in the high concentration zone are larger than that in the final state. These results demonstrate that the aggregation effect in the low concentration zone is much better than that in the high concentration zone.

Combing the experimental concentration data and Eq. 3, the removal efficiencies for all size ranges can be calculated, and the evaluated results are listed in Table 2. The removal coefficients in the low concentration zone are all larger than that in the high concentration zone. The former variation velocity of efficiency is larger than that for the later. The negative values in the size range of 0.3–1.0 μm demonstrate the concentration increase characteristic in the high concentration zone. For each size range, the aerosol number rates of high/low concentration zones are respectively about 1.8 (0.3–0.5 μm), 2.1 (0.5–1.0 μm), 5.6 (1.0–2.5 μm), 7.2 (2.5–5.0 μm), 8.7 (5.0–10 μm), 8.0 (>10 μm). Further, at the end of experiment, the removal coefficients all reach the values larger than 82%, near the previous minimum of 85.9%. Nevertheless, here the efficiency range is 82.3% - 88.5%.

3.1.2. Aerosol deposition

Fig. 5 shows the macro and micro deposition aggregated on the inner surface of waveguide. With the action of acoustic field, a layer of carmine deposition is adhered on the bottom of transparent glass plate. The transparency degree of plate represents the severe extent of

Table 2
The evaluation for aerosol removal coefficient.

Aerosol size distribution (μm)	Removal coefficient (%)					
	0.3–0.5	0.5–1.0	1.0–2.5	2.5–5.0	5.0–10	>10
Low concentration zone at 23 min	36.5	46.5	85.4	94.6	96.1	97.1
High concentration zone at 23 min	−15.5	−14.2	17.6	61.1	65.9	76.7*
Final state	82.3	82.4	82.7	84.5	84.9	88.5
The previous work [17]	85.9	88.9	97.7	99.1	88.5	99.7

* Negative values indicates the increase of number concentration.

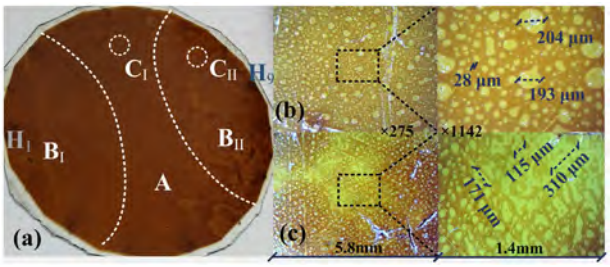

Fig. 5. The deposition distribution. (a) Macrograph, (b) and (c) electron microscope respectively in zone C_I and C_{II}.

acoustic sedimentation process for the aerosols. As shown in Fig. 5a, the high (in zone A) and low (in zone B_I and B_{II}) transparency zones on plate approximately constitute the shape of "I", similar to the shape of aerosol concentration distribution analyzed in Section 3.1.1. The lower transparency in zones of B_I and B_{II} compared with the zone A demonstrates the deposition in zone A is seemingly thicker than that in zone B. Such thickness difference indicates the extent of aerosol aggregation and sedimentation process in zone A is much severer than that in zone B.

Fig. 5 b and c respectively shows the micro deposition characteristic of the thick zone C_I and the thin zone C_{II}. The thick deposition layer in Fig. 5b consists of the conjoint agglomerates with dispersed spacing pieces of size about 28–204 μm. The thin deposition layer in Fig. 5c consists of the dispersed agglomerates with spacing of size about 115–310 μm.

Fig. 6 shows the detail characteristic of thick deposition in zone C_I. A layer of small tabular solid aggregates are covered on the surface of waveguide. As shown in Fig. 6a, the size range of small tabular aggregate is about 1.668–6.01 μm. With larger magnification in Fig. 6b, the surface of small aggregate has regular grooves of size range about 394.6–1296 nm, and the edges of grooves in Fig. 6c are covered with aggregate particles of sizes 67.08–210.1 nm. These large particles are comprised of nanoparticles 11.12–20.7 nm, as shown in Fig. 6d.

3.2. Acoustic field and its relation to aerosol aggregation

Fig. 7 shows the characteristic of acoustic field in simulation and experiment under the operating condition of mode 1. As the instantaneous sound pressure of intensity in the range of −0.22 to 1 is divided into 18 equal parts, the simulated pressure distribution is displayed in Fig. 7a. This division quantifies the structure of acoustic field corresponding to fluctuation regulation. The acoustic field structure reveals the specific distribution pattern with two symmetrical sections. Around the center of distribution, the symmetrical pattern is the shape of "I" similar to the aggregation pattern analyzed in Section 3.1. Combing with the experimental wavepackets [17] in Fig. 7c, the pressure fluctuation extent at the position near HSS is much greater than that at the position far away HSS. Attributing to the complex chemical smog aerosol with the acoustic radiation force regime equation 2, the solely obvious pressure gradient between the positions x_3 and x_6 causes numerous aerosols in the anti-neck [17] zone around x_5. For the acoustic field

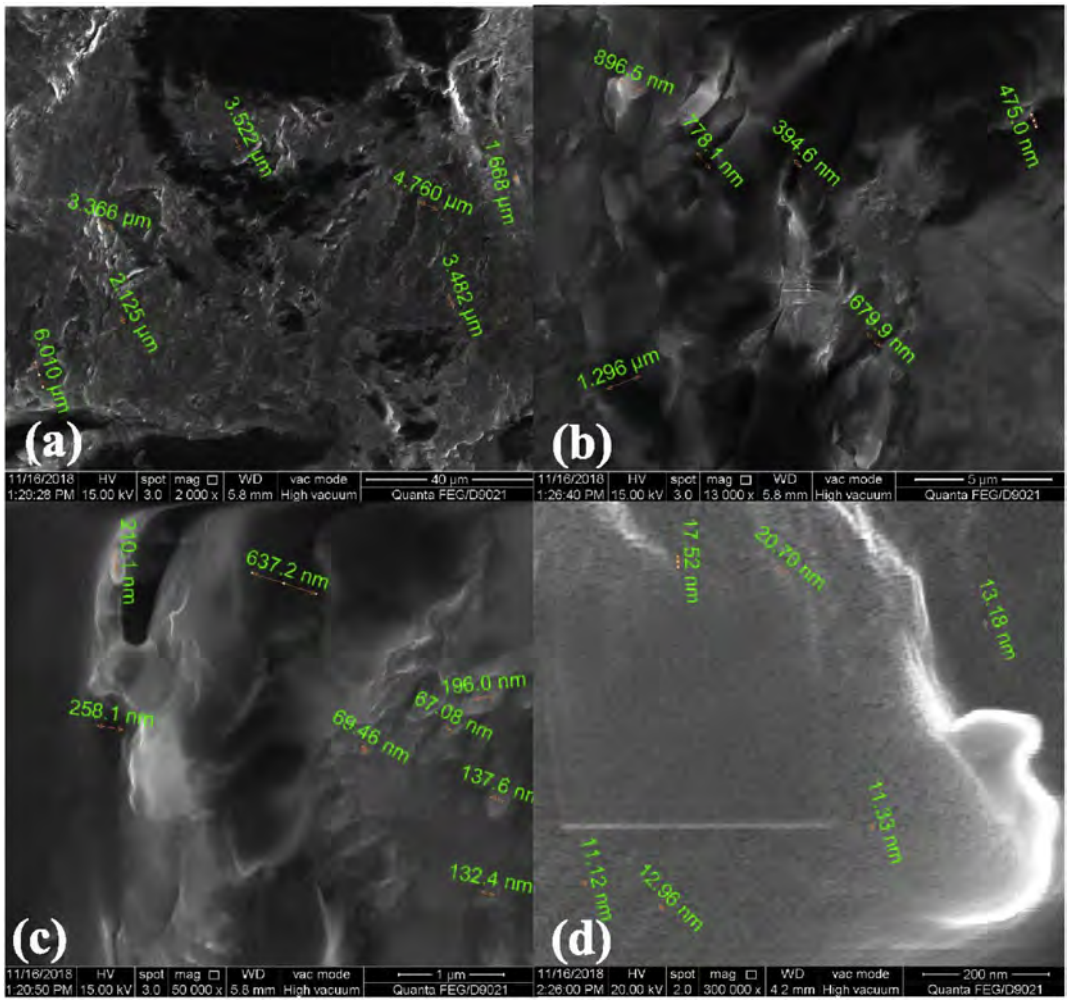

Fig. 6. The SEM image of aggregate. (a), (b), (c) and (d) correspond to different magnifications.

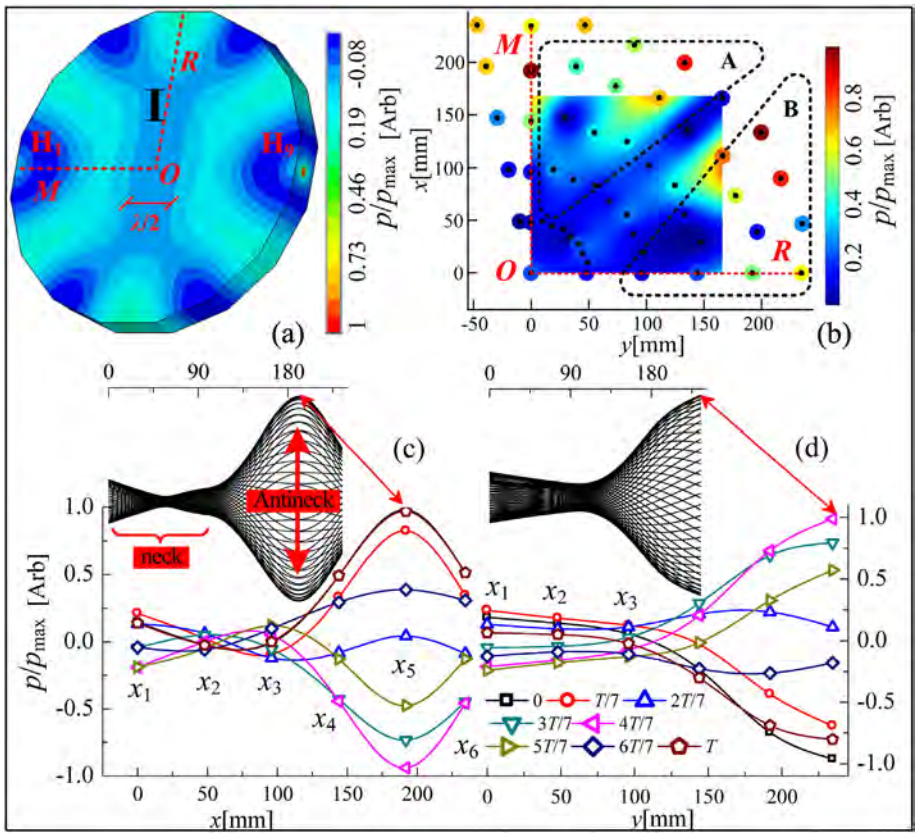

Fig. 7. The distribution of sound pressure. (a) And (b) respectively refer to the simulated and experimental results; (c) and (d) respectively refers to the experimental wave packets along *OM* and *OR*.

between x_1 and x_3, the actual geometry of neck instead of dot [19] causes the few aerosols in the neck zone.

Using the sound pressure amplitude at each position measured within quarter plane of *MOR*, the experimental pressure distribution is displayed in Fig. 7b. It can be seen that the experimental distribution is similar to the simulated distribution. While numerous aerosols exists in the strength acoustic filed A, the week acoustic field B results in the few aerosols and thick deposition. The similarly low sound pressure along *OR* in Fig. 7b and the similarly week pressure gradient between x_1 and x_3 in Fig. 7d simultaneously cause the similar thickness in the whole deposition zone A in Fig. 5a. Such manipulation effect should derive from the strong aggregation, sedimentation and removal based on the secondary radiation force [17].

The structure similarity of pattern I in Figs. 3, 5a and 7a demonstrates the equal pressure pattern in the middle of simulated distribution quantifies similarly the specific size of pattern I for aerosol aggregation effect. For conveniently weighing the size, as shown in Fig. 7a, one equal pressure pattern is defined as the main characteristic length *a*, where $a = \lambda/2$ (half wavelength). This characteristic length is two times than the experimental value λ/4 shown in Fig. 3. Even though that, large characteristic length causes large size of pattern I and better aerosol aggregation, especially the excellent removal effect in the low concentration zone.

3.3. The effective aggregation in other three operating modes

Fig. 8 shows the aerosol aggregation patterns caused by symmetrically opposing acoustic fields with two, four and eight pairs of resonators. Just as the relation between aerosol pattern and simulated acoustic field analyzed in Section 3.2, the experimental aerosol aggregation effect shown in Fig. 8 a~c perfectly corresponds to the simulated acoustic filed structure shown in Fig. 8 d~f under the operating conditions. The high concentration zones for aerosols constitute the specific patterns with different aerosol petals. The number of petals equals to the pole number of operating HSS, and the number concentrations outside the aerosol petals are very low.

It is noteworthy that the effect of aerosol petal pattern shown in Fig. 8a very well agrees with the verified X-pattern effect [19] without regard of its aerosol aggregation chamber of square cavity. The previous reference [19] demonstrates that the pattern width in the four ends of X shape is close to zero. In contrast, here the end width of X shape pattern similarly equals to the side of normal 16-sided waveguide. The large width of the X-end indicates the edge number tuning method of the polygon aggregation chamber has potential in developing industrial numerous aerosol aggregation control technology. This aerosol tuning aspect has not been proposed in previous other aerosol control study.

Besides, depended on the symmetrical structure characteristic of aerosol pattern and acoustic field, the main areas for the aerosol removal and the annular pressure pattern in the middle of waveguide are determined simultaneously. Such simultaneity indicates the aerosol petal distribution in two-dimensional waveguide can be pre-designed by acoustic field simulation in the future improvement of aerosol technology. The technological use of acoustic field simulation decreases the complexity in the process of industrially manufacturing precise aerosol device. Furthermore, for the low concentration zone, the experimental characteristic length for aerosol removal area can be evaluated by the diameter of macro circle A. With the similar quantifying method about the simulated equal-pressure-pattern size for weighing aerosol aggregation, the characteristic length *a* stamped in Fig. 8 d~f indicates the simulated size of low concentration zone in circle A.

Fig. 9 shows the characteristic lengths of aerosol removal at four operating conditions. These similar values in experiment and simulation verify the feasibility of quantifying method. With the number increase of operating HSS, the characteristic length becomes gradually large. The maximum value is 1.5λ (16 poles), obviously larger than the

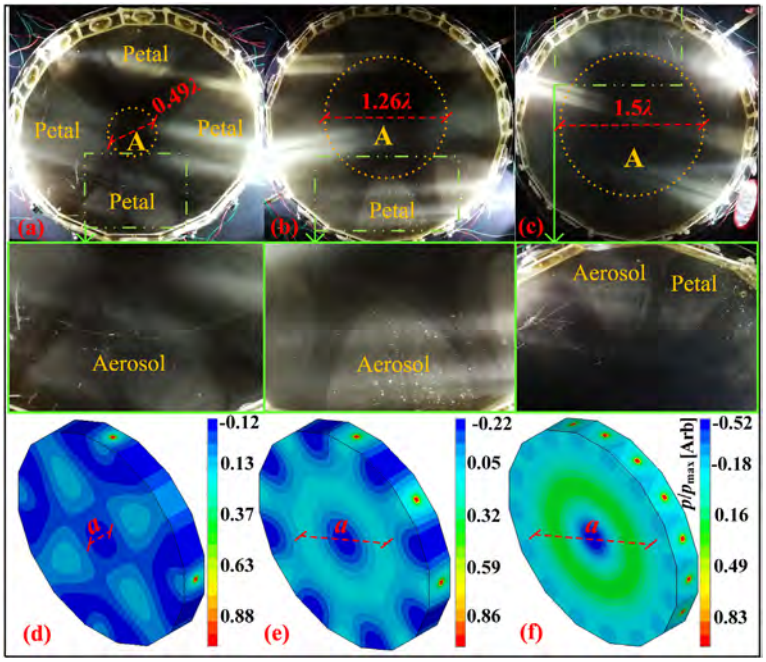

Fig. 8. The experimental manipulation and the simulated acoustic field. (a) And (d), (b) and (e), and (c) and (f) respectively refer to four, eight and sixteen HSS poles.

previous study of half-wavelength [19]. The maximum rate of characteristic length is 12 ($(1.5\lambda)/(\lambda/8) = 12$), compared to the one-dimension standing wave field where $a = \lambda/8$ [17]. The enlarged characteristic length verifies the operating number tuning method of multiple HSS has potential in the development of the industrial aerosol aggregation control technology. The middle variable between the operating number tuning and the aerosol control is the petal number and size of aerosol aggregation pattern.

Especially, referring to the comparison from 2 HSS poles to 16 HSS poles, the maximum rate of the removal areas in two different modes reaches 36 ($(1.5\lambda)^2/(0.25\lambda)^2 = 36$). The large removal area means the better aggregation effect, and the aggregation rate represented by the area rate achieves to 36. The big aggregation rate further indicates that the findings and methodology studied in this paper have specific potential in designing huge aerosol device used for submicronic particle emission control. The potential device should belong to the revolutionary aerosol technology. It can be predicted that the future industrial utilization in the workplace with aerosol emission might brought the eliminations of the occupational risk of worker [7] and the health risk of consumer [8]. With the hope of achieving this objective, several generations of researches should be encouraged to carry out further study [1].

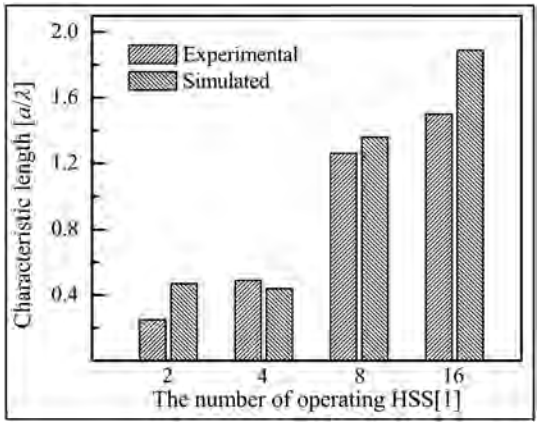

Fig. 9. The sizes of low concentration zone.

4. Conclusions

The aerosols aggregated through the symmetrically opposing acoustic filed modulated by the pole number of opposing HSS in normal 16-sided waveguide are studied. No-uniform two-dimensional acoustic standing wave fields in the four regular operating modes of working HSS are focused on both in experiment and simulation. The smog aerosol generated in the combustion of chemical material is used to display the aggregation effect. The initial amount percent of submicronic particles within the aerosols is about 75%, and the amount percent of $PM_{2.5}$ is about 91%. Results show that the aggregation effects of the acoustic field on the chemical smog aerosol are especially obvious. Under the operating mode of two poles, the patterns of aerosol concentration distribution, deposition and acoustic field structure are all simultaneously displayed as the shape of "I". For the inner of "I", the aerosol concentration is low; the deposition is thick, and the aerosol removal efficiency is much larger than that in the outside. At final state, the removal efficiencies for the aerosols of sizes >0.3 are about 82.3% - 88.5%. The nanoparticles (11.12–20.7 nm) in chemical smog constitute the deposition aggregates with regular grooves (394.6–1296 nm) on the surface of waveguide. The experimental patterns of aerosol distribution are the high/low concentration pattern with specific aerosol petals of number equaling to the pole number of operating HSS. The simulated pattern of acoustic field is similar to the experimental acoustic field, and it is also obviously similar to the experimental aerosol pattern. Due to the acoustic radiation force, the concentration near the center of waveguide is much lower than that near the side. The simulated equal-pressure-pattern around the center can represent the simulated removal effect. The effect in the operating condition of 16 pole HSS mode is 36 times than that in 2 pole HSS, and the characteristic length achieving to 1.5λ weighs the effective removal. The more the poles number is, the better the removal effect is. The aerosol aggregation effect in 16-sided waveguide can be regulated by tuning the operating number of symmetrically opposing HSS. The findings and methodology are a valuable

contribution to the area of aerosol control, particularly in the field of submicronic particles.

Declaration of Competing Interest

The authors declare that they have no conflict of interest.

Acknowledgements

This paper is supported by the Natural Science Research Project in Colleges and Universities in Jiangsu Province of China (Grants No 19KJB470022), the Natural Science Foundation of Jiangsu Province (Grants No BK20191019), and the Scientific Research Start-up Foundation funding of High-level Introduction Talents of Nanjing Institute of Technology (Grants No YKJ201912).

References

[1] D.B. Warheit, Hazard and risk assessment strategies for nanoparticle exposures: how far have we come in the past 10 years? F1000Research 7 (2018) 376, https://doi.org/10.12688/f1000research.12691.1.
[2] M. Morgeneyer, O. Aguerre-Chariol, C. Bressot, STEM imaging to characterize nanoparticle emissions and help to design nanosafer paints, Chem. Eng. Res. Des. 136 (2018) 663–674, https://doi.org/10.1016/j.cherd.2018.06.013.
[3] C. Bressot, A. Aubry, C. Pagnoux, O. Aguerre-Chariol, M. Morgeneyer, Assessment of functional nanomaterials in medical applications: can time mend public and occupational health risks related to the products' fate? J. Toxicol. Environ. Health 81 (2018) 957–973, https://doi.org/10.1080/15287394.2018.1477271.
[4] C. Bressot, N. Shandilya, T. Jayabalan, G. Fayet, M. Voetz, L. Meunier, O. Le Bihan, O. Aguerre-Chariol, M. Morgeneyer, Exposure assessment of nanomaterials at production sites by a short time sampling (STS) approach strategy and first results of measurement campaigns, Process Saf Environ. 116 (2018) 324–332, https://doi.org/10.1016/j.psep.2018.02.012.
[5] M. Morgeneyer, N. Shandilya, Y. Chen, O. Le Bihan, Use of a modified Taber abrasion apparatus for investigating the complete stress state during abrasion and in-process wear particle aerosol generation, Chem. Eng. Res. Des. 93 (2015) 251–256, https://doi.org/10.1016/j.cherd.2014.04.029.
[6] D. Gohler, M. Stintz, L. Hillemann, M. Vorbau, Characterization of nanoparticle release from surface coatings by the simulation of a sanding process, Ann. Occup. Hyg. 54 (2010) 615–624.
[7] C. Bressot, N. Shandilya, E.S. Da Costa Nogueira, A. Cavaco-Paulo, M. Morgeneyer, O. Le Bihan, O. Aguerre-Chariol, Exposure assessment based recommendations to improve nanosafety at nanoliposome production sites, J. Nanomater. (2015) https://doi.org/10.1155/2015/931405.
[8] M. Morgeneyer, A. Ramírez-Gómez, M. Poletto, S. Ward-Smith, R.J. Tweedie, J.Y.Y. Heng, S. Maass, C. Bressot, Particle technology as a uniform discipline? Towards a holistic approach to particles, their creation, characterisation, handling and processing! Chem. Eng. Res. Des. 146 (2019) 162–165, https://doi.org/10.1016/j.cherd.2018.11.029.
[9] J.A. Scales, R. Snieder, What is a wave? Nature 401 (1999) 739–740, https://doi.org/10.1038/44453.
[10] K. Melde, A.G. Mark, T. Qiu, P. Fischer, Holograms for acoustics, Nature 537 (2016) 518–522, https://doi.org/10.1038/nature19755.
[11] D. Kielpinski, QUANTUM PHYSICS Quantum sound waves stick together, Nature 527 (2015) 45–46.
[12] G. Zhang, T. Zhou, L. Zhang, J. Wang, Z. Chi, E. Hu, Improving acoustic agglomeration efficiency of coal-fired fly-ash particles by addition of liquid binders, Chem. Eng. J. 334 (2018) 891–899, https://doi.org/10.1016/j.cej.2017.10.126.
[13] G. Shen, X. Huang, C. He, S. Zhang, L. An, Experimental study of acoustic agglomeration and fragmentation on coal-fired ash with different particle size distribution, Powder Technol. 325 (2018) 145–150, https://doi.org/10.1016/j.powtec.2017.10.037.
[14] E.H. Brandt, Acoustic physics - suspended by sound, Nature 413 (2001) 474–475, https://doi.org/10.1038/35097192.
[15] Z. Qiao, W. Dong, Y. Huang, V. Naso, Effect of temperature tuning on the aerosol acoustic aggregation process, J. Environ. Sci. (China) 67 (2018) 161–170, https://doi.org/10.1016/j.jes.2017.08.021.
[16] Z. Qiao, Y. Huang, V. Naso, W. Dong, The advantage of aerosol manipulation by twin types of acoustic resonances, J. Clean Energy Tech. 5 (2017) 142–146, https://doi.org/10.18178/jocet.2017.5.2.359.
[17] Z. Qiao, Y. Huang, V. Naso, D. Wei, Aerosol manipulation through modulated multiple acoustic wavepackets with a pair of resonators, Powder Technol. 322 (2017) 24–31, https://doi.org/10.1016/j.powtec.2017.08.062.
[18] M. Cheng, W. Dong, Z. Qiao, Experimental study on structured complex acoustic field and its effectiveness of particle manipulation, J. Southeast Univ. (Nat. Sci. Ed.) 46 (2016) 720–726, https://doi.org/10.3969/j.issn.10010505.2016.04.008.
[19] Z. Qiao, Y. Huang, N. Vincenzo, W. Dong, Aerosol manipulation by acoustic tunable phase-control at resonant frequency, Powder Technol. 281 (2015) 76–82, https://doi.org/10.1016/j.powtec.2015.04.081.
[20] D. Zhou, Z. Luo, M. Fang, M. Lu, J. Jiang, H. Chen, M. He, Numerical calculation of particle movement in sound wave fields and experimental verification through high-speed photography, Appl. Energy 185 (2017) 2245–2250, https://doi.org/10.1016/j.apenergy.2016.02.006.
[21] F. Fan, X. Xu, S. Zhang, M. Su, Modeling of particle interaction dynamics in standing wave acoustic field, Aerosol Sci. Technol. 53 (2019) 1204–1216, https://doi.org/10.1080/02786826.2019.1652724.
[22] Q.J. Guo, Z.N. Yang, J.S. Zhang, Influence of a combined external field on the agglomeration of inhalable particles from a coal combustion plant, Powder Technol. 227 (2012) 67–73, https://doi.org/10.1016/j.powtec.2011.12.033.
[23] J.Z. Liu, G.X. Zhang, J.H. Zhou, J. Wang, W.D. Zhao, K.F. Cen, Experimental study of acoustic agglomeration of coal-fired fly ash particles at low frequencies, Powder Technol. 193 (2009) 20–25, https://doi.org/10.1016/j.powtec.2009.02.002.
[24] J.A. Gallego-Juarez, E. De Sarabia, G. Rodriguez-Corral, T.L. Hoffmann, J.C. Galvez-Moraleda, J.J. Rodriguez-Maroto, F.J. Gomez-Moreno, A. Bahillo-Ruiz, M. Martin-Espigares, M. Acha, Application of acoustic agglomeration to reduce fine particle emissions from coal combustion plants, Environ. Sci. Technol. 33 (1999) 3843–3849, https://doi.org/10.1021/es990002n.
[25] T.L. Hoffmann, Visualization of acoustic particle interaction and agglomeration: theory and experiments, J. Acoust. Soc. Am. 99 (1996) 2130, https://doi.org/10.1121/1.415400.
[26] P.S. LEE, M.T. CHENG, D.T. SHAW, The influence of hydrodynamic turbulence on acoustic turbulent agglomeration, Aerosol Sci. Technol. 1 (1982) 47–58, https://doi.org/10.1080/02786828208958578.
[27] E.N.D.C. ANDRADE, Phenomena in a sounding tube, Nature 127 (1931) 438.
[28] J. Yan, L. Chen, L. Yang, Combined effect of acoustic agglomeration and vapor condensation on fine particles removal, Chem. Eng. J. 290 (2016) 319–327, https://doi.org/10.1016/j.cej.2016.01.075.
[29] G. Zhang, Z. Ma, J. Shen, K. Zhang, J. Wang, Z. Chi, Experimental study on eliminating fire smokes using acoustic agglomeration technology, J. Hazard. Mater. 382 (2020) 121089, https://doi.org/10.1016/j.jhazmat.2019.121089.
[30] G. Zhang, L. Zhang, J. Wang, Z. Chi, E. Hu, A new multiple-time-step three-dimensional discrete element modeling of aerosol acoustic agglomeration, Powder Technol. 323 (2018) 393–402, https://doi.org/10.1016/j.powtec.2017.10.036.
[31] Y. Shi, J. Wei, J. Qiu, H. Chu, W. Bai, G. Wang, Numerical study of acoustic agglomeration process of droplet aerosol using a three-dimensional CFD-DEM coupled model, Powder Technol. 362 (2020) 37–53, https://doi.org/10.1016/j.powtec.2019.12.017.
[32] J. Zheng, Y. Li, Z. Wan, W. Hong, L. Wang, Modification of the agglomeration kernel and simulation of the flow pattern in acoustic field with fine particles, Powder Technol. 356 (2019) 930–940, https://doi.org/10.1016/j.powtec.2019.09.022.
[33] J. Yan, Q. Lin, S. Zhao, L. Chen, Effect of seed nuclei combined with acoustic field on fine particles removal, Powder Technol. 340 (2018) 8–16, https://doi.org/10.1016/j.powtec.2018.09.020.
[34] K. Kilikevičienė, R. Kačianauskas, A. Kilikevičius, A. Maknickas, J. Matijošius, A. Rimkus, D. Vainorius, Experimental investigation of acoustic agglomeration of diesel engine exhaust particles using new created acoustic chamber, Powder Technol. 360 (2020) 421–429, https://doi.org/10.1016/j.powtec.2019.09.057.
[35] M. He, Z. Luo, M. Lu, S. Liu, M. Fang, Effects of acoustic and pulse Corona discharge coupling field on agglomeration and removal of coal-fired fine particles, Aerosol Air Qual. Res. 19 (2019) 2585–2596, https://doi.org/10.4209/aaqr.2018.08.0306.
[36] Z. Gong, P.L. Marston, W. Li, Reversals of acoustic radiation torque in bessel beams using theoretical and numerical implementations in three dimensions, Phys. Rev. Appl. 11 (2019) https://doi.org/10.1103/PhysRevApplied.11.064022.
[37] T.A. Johansson, M. Kleiner, Theory and experiments on the coupling of two Helmholtz resonators, J. Acoust. Soc. Am. 110 (2001) 1315–1328, https://doi.org/10.1121/1.1394741.
[38] Q. Zhenghui, H. Yaji, D. Wei, Acoustic resonance characteristics of symmetric cylindrical waveguide with Helmholtz sound source[J], J. Southeast Univ. (Nat. Sci. Ed.) 44 (03) (2014) 579–584.
[39] G.D. Skotis, D.R.S. Cumming, J.N. Roberts, M.O. Riehle, A.L. Bernassau, Dynamic acoustic field activated cell separation (DAFACS), Lab Chip 15 (2015) 802–810, https://doi.org/10.1039/c4lc01153h.
[40] R. Hirayama, D.M. Plasencia, N. Masuda, S. Subramanian, A volumetric display for visual, tactile and audio presentation using acoustic trapping, Nature 575 (2019) 320–323, https://doi.org/10.1038/s41586-019-1739-5.